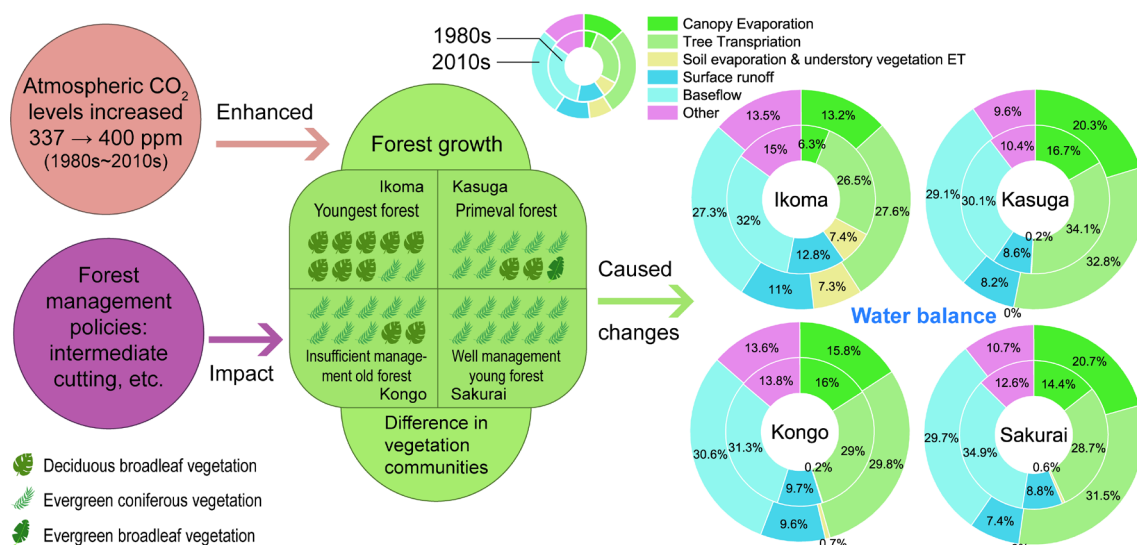


# Effects of Forest Growth in Different Vegetation Communities on Forest Catchment Water Balance

Kunyang Wang<sup>1</sup>, Shin-ichi Onodera<sup>2,\*</sup>, Mitsuyo Saito<sup>3</sup>, Yuta Shimizu<sup>4</sup>, Toru Iwata<sup>3</sup>

1. Graduate School of Integrated Arts and Sciences, Hiroshima University, 1-7-1 Kagamiyama, Higashi-Hiroshima-shi, Hiroshima, 739-8521, Japan
2. Graduate School of Advanced Science and Engineering, Hiroshima University, 1-7-1 Kagamiyama, Higashi-Hiroshima, 739-8521, Japan
3. Graduate School of Environmental and Life Science, Okayama University, 3-1-1 Tsushima-naka, Kita-ku, Okayama-city, Okayama, 700-8530, Japan
4. Western Region Agricultural Research Center, National Agriculture and Food Research Organization. 6-12-1 Nishifukatsu-cho, Fukuyama-shi, Hiroshima 721-8514, Japan



## ABSTRACT

Forest ecosystems are critical for adjusting the dynamic balance of the hydrological cycle. This balance is affected by vegetation community types, phenology, and forest density. Previous long-term catchment-scale model studies have focused on changes in forest

areas while ignoring the above factors. Since the 1980s, climate change caused by increases in atmospheric CO<sub>2</sub> levels has enhanced forest growth. Moreover, amendments to forest management policies, including intermediate cuttings caused by economic factors, have yielded unprecedented changes in forest ecosystems. In this study, we designed a methodology and created a credible model using the Soil and Water Assessment Tool (SWAT) that can precisely reflect water balance variations caused by different ecosystem situations during long-term changes in forest density. We focused on the Yamato River catchment in Western Japan, which includes three planted forests and one primeval forest, each markedly different with respect to vegetation community composition and management policy. In the process, we examined the ratio of coniferous vegetation and broad-leaved vegetation in different forest areas, used remote sensing methods to quantify the maximum and minimum leaf area index (LAI) of each forest region over 40 years, and calibrated the model by comparing the LAI growth curve, evapotranspiration, and streamflow with observed data. Moreover, we separated the decadal canopy evaporation, transpiration, and soil evaporation from the SWAT output results. We found that (1) forest evapotranspiration has increased in recent decades because of the above reasons; (2) in young or well-managed forests, the forest water balance may have changed significantly with forest growth. For long-term studies, it is necessary to distinguish the growth characteristics of different forests during different periods, and a detailed definition of a mixed forest is required. The forest parameters and growth characteristics are critical for understanding forest ecosystems and cannot be ignored at catchment-scale.

**Keywords:** Forest density, SWAT, remote sensing, evaporation, transpiration

## 1. Introduction

Forest ecosystems are vital for adjusting the dynamic balances of the hydrologic cycle, and usually cover the upstream regions of catchments. The water balance is affected by forest growth and management, both of which change the forest density, particularly the canopy density, which directly determines the canopy interception or storage capacity and forest evapotranspiration (ET) (Skovsgaard et al., 2011; Durlo et al., 2016; MacDicken et al., 2016; Sharma and Saikia, 2018). In addition, forest density also determines the water absorption capacity of the forest plants and impacts the soil water content and groundwater recharge process (Osman and Barakbah, 2006; Nepstad et al., 1994). An extreme case is the Amazon region, where the ET of the primeval forest is much higher than that of the young planted forest. This difference was most obvious in the canopy transpiration (Kunert et al., 2015).

During 1982 to 1999, global changes in climate of atmospheric CO<sub>2</sub> levels increased from 337 to 369 ppm, break through the limitation of temperature for plant growth and enhanced plant growth (Nemani et al. 2003). This kind of climate change is still going on, the atmospheric CO<sub>2</sub> levels have exceeded 400 ppm at the second half of 2010s (Quéré et al. 2015). This changes the forest ecosystem and environment from a stable situation.

In addition, due to global economic growth, forest management policies driven by economic factors have also led to changes in forest density (Takeda et al., 2010; Rautiainen et al., 2011). Since 1990, the area of primeval forest has continuously decreased in South America and Africa; however, the area of planted forest increased by 123 million ha worldwide. These increases were particularly obvious in Asia and Europe (FAO, 2020). Until now, more than 2 billion ha of forest has management plans, while ~1.9 billion ha of forest is used primarily for production (FAO, 2020). Thus, intermediate cutting has a significant impact on the forest ecosystem and environment.

Based on the above factors, forest ecosystems have likely undergone major changes since

the 1980s, which can affect the water balance at forest and catchment scales. However, the impact of forest growth and forest management on water balance has not been comprehensively analyzed in the context of long-term catchment-scale studies.

Changes in forest phenology also impact forest water balance, particularly between different vegetation communities such as coniferous and broad-leaved forests (Staelens et al., 2011; Paul-Limoges et al., 2020). Under the same climatic and latitude conditions, some studies note that the ET of coniferous forests is higher than that of broad-leaved forests because the coniferous forest canopy can intercept more precipitation during the winter (Swank and Douglass, 1974; Komatsu et al. 2008). However, some studies have found that broad-leaved forests exhibit higher ET because precipitation during the winter is generally low, and canopy interception differences during the winter are not important for annual ET (Komatsu et al., 2007; Komatsu et al., 2009). In the mid-latitudes, forests typically contain a mix of coniferous and broad-leaved vegetation. The compositions of the vegetation communities in different mixed forests vary, but this compositional difference is typically either underestimated or ignored in most studies.

Research on the forest hydrological cycle is currently limited, particularly studies of ET. Field work cannot currently obtain historical forest information; however, remote sensing technology has been a popular method used in recent years, with moderate resolution imaging spectroradiometer (MODIS) data as an example. MODIS enables direct access to leaf area index (LAI) and ET data. However, the spatial resolution of the ground data used by MODIS is 500 m (Running et al., 2019). At this scale, land-use types are typically mixed and do not include only forests. In addition, MODIS data are only available after 2000; therefore, they are not feasible for use in studies of long-term variations. Landsat imagery is another satellite-based remote sensing method. Landsat images are available from 1972 onwards, and due to frequent equipment replacements early on, the data after 1982 are higher quality. Unmanned aerial vehicle remote sensing is also a popular method, as it has

the advantage of extremely high spatial resolution; however, only recent data are available. For ET estimation, the simplest method subtracts river discharge from the precipitation amount; however, this method ignores transmission loss (Kayane and Takeuchi, 1971). Another method utilizes a potential ET equation, such as the Penman–Monteith, Priestley–Taylor, or Hargreaves ET equation, but only determines potential ET (Monteith, 1965; Priestley and Taylor, 1972; Hargreaves et al., 1985).

Hydrological models can be used to estimate the forest hydrological cycle. However, users do not have a sufficient number of forest type choices, as the options usually include only evergreen, deciduous, and mixed forests. In addition, the phenological characteristics of the different forest vegetation communities are also difficult to distinguish, which limits investigations of the effects of mixed forests with different vegetation communities on the water balance. The objective of this study was to build a credible SWAT model to address how ET (including canopy evaporation, transpiration, and soil evaporation) is influenced by the detailed temporal evolution of forest growth and management in different vegetation communities.

## 2. Materials and methods

### 2.1 Study catchment

The Yamato River catchment covers 1077 km<sup>2</sup> and had an average annual precipitation of ~1400 mm over the last 50 years. Forests cover over 40% of the catchment and are located in mountains with slopes greater than 30°. The mountainous areas are primarily dominated by Dystric Regosols. The forests in the Yamato River catchment are predominately planted forests. Four forest regions are located within the catchment, each of which located on the mountains surrounding the Nara plain (Figure 1), and the distributions of the vegetation communities in the four forest regions also vary. We investigated the forest management history and the compositions of vegetation communities in each forest region.

Mt. Ikoma is located to the northwest of the Nara plain. Its primary vegetation type is *Quercus serrata*, which covers 78% of the forest region. Evergreen coniferous vegetation (*Cryptomeria japonica* and *Chamaecyparis obtuse*) covers 14% of the Ikoma forest region. The other 8% of the Ikoma forest region contains shrubs and bamboo forests. The ecosystems of the Ikoma forest region were destroyed by forest fires in the 1960s, and large-scale tree planting activity has gradually restored the forest ecosystem since the 1970s (Osaka Prefecture, 2021).

Mt. Kasuga is located to the northeast of the Nara plain. Its primary vegetation includes *Cryptomeria japonica* and *Chamaecyparis obtuse*, which cover 70% of the forest region. *Quercus serrata* covers 16% of the Kasuga forest region, while 14% of the forest is *Castanopsis cuspidate*, which is a broad-leaved evergreen vegetation type. Unlike the other forest regions, the Kasuga forest region is primeval forest (Nara Prefecture, 2016).

Mt. Kongo is located to the southwest of the Nara plain. Its primary vegetation includes *Cryptomeria japonica* and *Chamaecyparis obtuse*, which cover 83% of the forest region. *Quercus serrata* covers 14% of the Kongo forest region, while 3% of the forest is shrubs and bamboo forests. This forest area has a small timber mill, but trees usually grow freely due to limited management conditions such that 80 year old trees accounted for a large proportion of the forest in recent years (Tomimura Environmental Office, 2015; Japan Foreststock Association, 2021).

The final forest region is located around the Sakurai and Yoshino forest regions southeast of the Nara plain (hereafter the Sakurai forest region). Because 97% of the Sakurai forest region is dominated by *Cryptomeria japonica* and *Chamaecyparis obtuse*, the region is considered to be an evergreen coniferous forest. This forest region is well managed, and is an important timber producing area of Japan, from which trees greater than 50 years old are cut down for timber (Nara Prefecture, 2021). Due to economic reasons, felling and tree planting activities occurred most frequently during the 1960s and 1970s in this region (Agriculture and Forestry Department of Nara, 2018).

## 2.2 Soil and Water Assessment Tool

SWAT is a scale model developed by the United States Department of Agriculture (USDA, 1980). SWAT is not only effective for evaluating surface water, but also plays a vital role in baseflow analyses (Sun and Cornish, 2005; Marhaento et al., 2017), demonstrating that SWAT can comprehensively analyze water balance. SWAT simulates the canopy interception, infiltration, ET, soil water, surface runoff, groundwater recharge, and streamflow in a region. The water balance equation that governs the land phase of the hydrological cycle in the SWAT is expressed as (Neitsch et al., 2011):

$$SW_t = SW_0 + \sum_{i=1}^t (R_{day} - Q_{surf} - E_a - W_{seep} - Q_{gw}) \quad (1)$$

where  $SW_t$  is the final soil water content (mm H<sub>2</sub>O),  $SW_0$  represents the initial soil moisture (mm H<sub>2</sub>O),  $t$  is time (d),  $R_{day}$  is the daily precipitation (mm H<sub>2</sub>O),  $Q_{surf}$  is the accumulated excess runoff or rainfall (mm H<sub>2</sub>O),  $E_a$  is the amount of ET (mm H<sub>2</sub>O),  $W_{seep}$  is the amount of water entering the vadose zone from the soil profile (mm H<sub>2</sub>O), and  $Q_{gw}$  is the amount of return flow (mm H<sub>2</sub>O).

The SWAT provides a variety of calculation methods for potential ET. In this study, we used the Penman–Monteith equation to calculate ET, which is expressed as (Monteith, 1965):

$$\lambda E = \frac{\Delta \cdot (H_{net} - G) + \rho_{air} \cdot c_p \cdot [e_z^0 - e_z] / r_a}{\Delta + \gamma \cdot (1 + r_c / r_a)} \quad (2)$$

where  $\lambda E$  is the latent heat flux density (MJ m<sup>-2</sup> d<sup>-1</sup>),  $E$  is the depth rate evaporation (mm d<sup>-1</sup>),  $\Delta$  is the slope of the saturation vapor pressure–temperature curve (kPa °C<sup>-1</sup>),  $H_{net}$  is the net radiation (MJ m<sup>-2</sup> d<sup>-1</sup>),  $G$  is the heat flux density to the ground (MJ m<sup>-2</sup> d<sup>-1</sup>),  $\rho_{air}$  is the air density (kg m<sup>-3</sup>),  $c_p$  is the specific heat at a constant pressure (MJ kg<sup>-2</sup> °C<sup>-1</sup>),  $e_z^0$  is the saturation vapor pressure of the air at height  $z$  (kPa),  $e_z$  is the water vapor pressure of the air at height  $z$  (kPa),  $\gamma$  is the psychrometric constant (kPa °C<sup>-1</sup>),  $r_c$  is the plant canopy resistance (s m<sup>-1</sup>), and  $r_a$  is the diffusion resistance of the air layer (aerodynamic resistance) (s m<sup>-1</sup>). Further details regarding the water balance and ET equations

can be found in the SWAT documentation (Neitsch et al., 2011).

There are many parameters available in the plant growth database, and forest growth characteristics can be defined sufficiently in the SWAT plant growth database using these parameters. The most critical parameters are the LAI parameters. By controlling the growth characteristics and maximum LAI, SWAT can calculate the annual LAI vegetation changes and use this value to calculate the canopy water storage, as illustrated by Equation 3 (Neitsch et al., 2011):

$$can_{day} = can_{mx} \cdot \frac{LAI}{LAI_{mx}} \quad (3)$$

where  $can_{day}$  is the maximum amount of water that can be trapped in the canopy on a particular day (mm H<sub>2</sub>O),  $can_{mx}$  is the maximum amount of water that can be trapped in the fully developed canopy (mm H<sub>2</sub>O), LAI is the leaf area index for a particular day, and  $LAI_{mx}$  is the maximum leaf area index of the plant.

The plant growth modes in SWAT are designed for crops and are unsuitable for perennial vegetation, such as forest trees. In this study, we applied SWAT-T, which is a revised version of SWAT, modified the growth process of perennial vegetation, and more suitable for forest catchment than the original version (Alemayehu et al., 2017).

### 2.3 General Data Processing

SWAT requires topography, land use, and soil data to determine the hydrologic response units (HRUs) for the watershed configuration. The topography data were obtained from the Shuttle Radar Topography Mission of the United States Geological Survey, which has a spatial resolution of 30 m. Land use and soil data were obtained from the Ministry of Land, Infrastructure, Transport and Tourism of Japan, which has a spatial resolution of 100 m. The slope data were calculated from the digital elevation model data. Land use maps utilized the following categories: agricultural land, residential land, forests, grassland, and wasteland. The spatial datasets were converted to SWAT input



datasets using ArcSWAT 10.6, an external Geographical Information System interface (Neitsch et al., 2011) and the SWAT version used was 2012. The climate data were derived from eight meteorological stations located in or close to the watershed (Figure 1) and included daily precipitation, maximum temperature, minimum temperature, wind speed, solar radiation, and relative humidity data. We obtained 40 years of streamflow data in the downstream areas of each forest regions (Figure 1). Banjou station covered the Kasuga forest region, Hota station covered the Sakurai forest region, Ouji station covered the Ikoma region and the two upstream forest regions, and Kashiwara station covered the entire forest area. For global calibration period, we collected MODIS ET data for each forest region to improve the model efficiency. The forest types were not distinguished in our original land use map, which is similar to the land use maps of most studies. Therefore, in this study, we classified the forest region types using the method described in section 2.4.

## 2.4 Forest Data Processing

We first created a plant growth database for the studied forest region. Most of the parameters were directly referenced from previous studies or field survey results. CN2, which reflects the land cover surface characteristics, is affected by the soil hydrological group, land cover type, and land cover density. In this study, we calculated the deciduous forest to evergreen forest area ratios in the forest regions and the initial CN2 for each forest type to obtain the CN2 value of each forest area for the various hydrological groups (Soil Conservation Service Engineering Division, 1986), as follows:

$$CN2_i = CN2_{di} \cdot a_d + CN2_{ei} \cdot a_e \quad (4)$$

where  $CN2_i$  is the CN2 of hydrological group  $i$ ;  $CN2_{di}$  and  $CN2_{ei}$  are the CN2 values of hydrological group  $i$  in deciduous and evergreen forests, respectively; and  $a_d$  and  $a_e$  are the proportions of deciduous and evergreen forests compared to the total forest region, respectively. The CN2 values required calibration via the SWAT calibration and uncertainty procedure (SWAT-CUP).

The second step required calculating the leaf area development curve parameters for each forest region. The canopy characteristics of the vegetation growth stage were reflected by FRGRW1, LAIMX1, FRGRW2, and LAIMX2, as listed in Table 1. The first growth point was before the vegetation entered the rapid growth season, and the second growth point was after the rapid growth season and before reaching the maximum LAI (Neitsch et al., 2011). These parameters were based on the MODIS LAI product and calibrated and validated using a daily time step (Myneni et al., 2015) in SWAT-CUP. The LAI data used for calibration was the average of all sampling points in the forest region collected on the same date. The fitted parameters were used in the SWAT for all periods, (Table 1).

The third step involved setting the minimum and maximum LAIs for each period. In SWAT, the minimum LAI parameters are LAI\_INIT and ALAI\_MIN, and the maximum LAI parameter is BLAI. These parameter values were calculated from the MODIS LAI and the Landsat normalized difference vegetation index (NDVI). The values for the 2000s and 2010s were obtained directly using MODIS LAI products, while the values during the 1980s and 1990s were calculated using Equation 5:

$$LAI_h = \frac{LAI_{modis}}{NDVI_{landsat}} \cdot NDVI_h \quad (5)$$

where  $LAI_h$  is the historic minimum or maximum LAI in the 1980s and 1990s,  $LAI_{modis}$  is the average MODIS LAI of a particular sampling point and month for different years during the 2000s and 2010s,  $NDVI_{landsat}$  is the average Landsat NDVI for a particular sampling point and month for different years during the 2000s and 2010s, and  $NDVI_h$  is the historic Landsat NDVI of a particular sampling point and month for different years during the 1980s and 1990s. We utilized multiple sampling points in each forest region, and the maximum or minimum value for each period was the average value of all the sampling points for all years during the period. ALAI\_MIN, LAI\_INIT, and BLAI did not require calibration in SWAT-CUP (Table 3).

## 2.5 Model Implementation

Model calibration and validation were divided into two stages. The first stage calibrated the canopy growth processes of the forest phenology characteristics. The default operation schedule setting was that plant growth begins in May and ends (withers) in August, and the plant LAI was set to 0 before growth began and after withering. This setting is completely different from the actual scenario, particularly for forests that exhibit high evergreen vegetation community coverage. To improve upon this unreasonable setting, two adjustments must be made to the forest operation schedule. The initial growth date was adjusted to January 1<sup>st</sup> and the wither data was adjusted based on the actual scenario; thus, the wither operation was set to “harvest only” as the default operation. Because the default wither operation is “harvest and kill,” the LAI is set to 0 after this operation. By setting the default to “harvest only,” the LAI after this operation is set to the ALAI\_MIN. Thus, we can define the LAI of the dormant period using the LAI\_INIT and ALAI\_MIN values and adjust the growth process using the canopy growth parameters. This stage calibrates four plant growth parameters (FRGRW1, LAIMX1, FRGRW2, and LAIMX2) and two growth temperature parameters (T\_OPT and T\_BASE). In this stage, simulations were run in daily time steps to compare the model results with the observed MODIS LAI data, with calibration using the 2017 data and validation using the 2018 data. The model was then adjusted based on the fitted plant growth parameters after calibration and validation.

In the second stage, simulations were run in monthly time steps. The research period was divided into four 10 y sub-periods. Parameters unrelated to forest hydrological processes, such as soil characteristics, were only calibrated once during the global calibration period using methods from previous studies to avoid the influence of changing parameters and land use impacts such as urbanization (Wang et al., 2021). Parameters related to forest hydrological processes (CANMX and

ESCO) of the forest HRU, must be re-calibrated for each sub-calibration period because the forest scenario changed in each period. The same initial range of ESCO was applied to all periods and forest regions, while the range of the maximum canopy storage (CANMX) was allowed to vary.

In this study, we used a range of 0.5–1.5 times the calculation result of Equation (6) as the initial range of CANMX for each sub-calibration period in each forest region (Von Hoyningen-Huene, 1981), which is widely used in forest and ET studies (Kozak et al., 2007; Dube et al., 2017).

$$can_{mx} = 0.935 + 0.498(LAI_{mx}) - 0.00575(LAI_{mx}^2) \quad (6)$$

To determine the reliability of the results obtained from the simulation, it was necessary to evaluate their accuracy. In this study, three indices were chosen to ascertain the reliability of the results: the coefficient of determination ( $R^2$ ), the Nash–Sutcliffe efficiency (NSE) (Nash and Sutcliffe, 1970), and the percentage of bias (PBIAS) (Equations 7–9, Kvalseth, 1985; Nash and Sutcliffe, 1970; Gupta et al., 1998).

$$R^2 = \frac{\sum_i [(X - X') (Y - Y')]^2}{\sum_i (X - X')^2 \sum_i (Y - Y')^2} \quad (7)$$

$$NSE = 1 - \left[ \frac{\sum_i (X - Y)^2}{\sum_i (X - X')^2} \right] \quad (8)$$

$$PBIAS = \frac{\sum_i (X - Y)}{\sum_i X} \times 100 \quad (9)$$

where  $X$  is the observed data;  $Y$  is the result of the SWAT simulation;  $X'$  and  $Y'$  are the means of the observed and simulated data, respectively; and  $i$  is the number of observed or simulated data points.  $R^2$  ranges between 0 and 1, with larger values indicating better model simulation performance. NSE is the most popular hydrological model efficiency indicator and ranges between  $-\infty$  and 1, where  $NSE = 1$  is the optimal value. The PBIAS is used to measure the difference between the simulated and measured values, and has an optimal value of zero. Positive and negative values indicate model estimation biases due to underestimation or overestimation, respectively.  $R^2$  and NSE values greater than 0.5 and an absolute value of  $PBIAS < 25$  are considered “satisfactory” simulation results, while

$R^2$  and NSE values greater than 0.75 and an absolute value of PBIAS < 10 are considered “very good” simulation results (Moriassi et al., 2007).

We also simulated a scenario after calibration and validation that applied the climate data from the 2010s to the forest scenario during the 1980s to assess the forest growth impact on water balance under the same climatic conditions.

## 2.6 Canopy Evaporation, Transpiration, and Soil Evaporation Estimations

To understand the changes in the forest hydrological processes, we separated the canopy evaporation ( $E_{can}$ ), transpiration ( $T$ ), and soil evaporation and the understory vegetation evapotranspiration ( $E_s$ ) in the forest regions. We separated the ET processes in the SWAT output results using Equations (10–21).

1) The actual free water held in the canopy was calculated using:

$$\text{if } R_{day} + can_0 \geq can_{day} : can_t = can_{day} \quad (10)$$

$$\text{if } R_{day} + can_0 < can_{day} : can_t = R_{day} + can_0 \quad (11)$$

where  $can_0$  is the remaining canopy water from the previous day after canopy evaporation (mm H<sub>2</sub>O) and  $can_t$  is the canopy water stored on the studied day (mm H<sub>2</sub>O).

2) The canopy evaporation was calculated:

$$\text{if } can_t \geq ET_{day} : E_{can} = ET_{day}, can'_0 = can_t - ET_{day}, ET' = 0 \quad (12-14)$$

$$\text{if } can_t < ET_{day} : E_{can} = can_t, can'_0 = 0, ET' = ET_{day} - E_{can} \quad (15-17)$$

where  $ET_{day}$  is the daily ET in the forest HRUs (mm H<sub>2</sub>O),  $E_{can}$  is the canopy evaporation (mm H<sub>2</sub>O),  $can'_0$  is the remaining canopy water (mm H<sub>2</sub>O), and  $ET'$  is the daily ET after canopy evaporation (mm H<sub>2</sub>O).

3) Transpiration was estimated ( $ET' > 0$ ):

$$\text{if } LAI \geq 3 : T = ET', E_s = 0 \quad (18 \text{ and } 19)$$

$$\text{if } LAI < 3: T = ET' \cdot \frac{LAI}{3}, E_s = ET' - T \quad (20 \text{ and } 21)$$

where  $T$  is the tree transpiration (mm H<sub>2</sub>O) and  $E_s$  is the soil evaporation and understory vegetation evapotranspiration (mm H<sub>2</sub>O).

### 3. Results

#### 3.1 Model Performance

To allow the forest LAI growth curve to conform to actual forest phenological changes, we calibrated FRGRW1, LAIMX1, FRGRW2, LAIMX2, T\_OPT, and T\_BASE at the HRU-scale in each forest region. The simulation results are shown in Figure 2, and the efficiency coefficients are listed in Table 2. The LAI during the dormant period of the default scenario was 0 and the maximum LAI was less than 3, which differ from those of the actual situation. The calibrated LAI growth curves were closely fitted to the actual forest phenology changes. The  $R^2$  and NSE values for all of the forest regions were greater than 0.9, and the absolute value of PBIAS was less than 2%.

In this study, a total of 18 parameters were calibrated to simulate ET and streamflow. CANMX and ESCO exhibited different fitting values in the sub-calibration periods. The fitted values for the different sub-calibration periods were verified in the corresponding sub-validation periods. The simulation results are shown in Figures 3 and 4, and the ET and streamflow efficiency coefficients are listed in Table 2.

The  $R^2$  and NSE values of the simulated ET results were greater than 0.8 and the absolute value of PBIAS was less than 5%, while the  $R^2$  of the simulated streamflow results was higher than 0.6, the NSE was greater than 0.55, and the absolute value of PBIAS was less than 15% (Table 2). Based on the modeling standards of Moriasi et al. (2007), all of the simulated results were “satisfactory.” At the Ouji and Kashiwara stations, the simulated results were “good,” and some periods were “very good.” At the Banjou station during the 1990s–2010s, the simulated results were “good.” Thus, the

overall modeling results can be considered reliable.

### 3.2 Forest Growth Impacts on Water Balance

We estimated the decadal ET processes for each forest region in the study area. During the study period, the total ET increased by 194 mm, 77 mm, 91 mm, and 178 mm in the Ikoma, Kasuga, Kongo, and Sakurai forest regions (Figure 5). Comparing the simulation scenario to the 2010s, the total ET increased by 131 mm, 32 mm, 17 mm, and 124 mm in the Ikoma, Kasuga, Kongo, and Sakurai forest regions, respectively, under the same climatic conditions. This change in the water balance is because forest growth includes both the impacts of long-term global climate change and anthropogenic forest management for economic reasons.

Canopy evaporation was the ET component that exhibited the most significant changes. Compared to the simulated scenario, canopy evaporation increased by 115 mm, 52 mm, -3 mm, and 93 mm in the Ikoma, Kasuga, Kongo, and Sakurai forest regions, respectively, under the same climatic conditions. The canopy evaporation in the Kasuga, Kongo, and Sakurai forest regions were higher than that in the Ikoma forest region.

Transpiration increased by 19 mm, 12 mm, and 41 mm in the Ikoma, Kongo, and Sakurai forest regions, respectively, under the same climatic conditions, but decreased by 18 mm in the Kasuga forest region. The soil evaporation and understory vegetation ET of the three evergreen vegetation forests were very low, but were high in the Ikoma forest region (average 122 mm) during the study period. It is worth noting that  $E_s$  only increased and  $E_{can}$  only decreased in the Kongo forest region under the same climatic conditions.

Under the same climatic conditions and with an increased ET, the surface runoff and baseflow from the forest decreased (Figure 6). Surface runoff decreased by 30 mm, 5 mm, 3 mm, and 20 mm in the Ikoma, Kasuga, Kongo, and Sakurai forest regions, respectively. Baseflow in these

regions decreased by 76 mm, 15 mm, 11 mm, and 76 mm, respectively. Although the baseflow quantity decreased, the proportion of lateral flow in the baseflow increased, particularly in the Ikoma and Sakurai forest regions, where the percentages of lateral flow in the baseflow were 24.7% and 23.3% and increased by 3.6% and 3.4%, respectively.

## 4. Discussion

### 4.1 Model Improvements and Uncertainty

The simulation results during the non-flood season were improved in this study compared to previous studies. Parajuli et al. (2018) compared MODIS ET and SWAT ET, and although the efficiency coefficients of the models reached reliable levels, their fitting results during the winter were insufficient. By adjusting the LAI growth curve to fit the actual situation, the blank period of the default setting caused by the “harvest and kill” operation was removed. During the non-flood season, the baseflow may be too low/too high due to too much/too little ET, respectively (Qin et al., 2009; Zhao et al., 2015). This is because the default LAI value is 0 during the blank period and some parameters may not be fully calibrated; thus, the ET and streamflow during the non-flood season may be higher or lower than the actual situation.

In this study, we calculated the initial CANMX range before calibration based on the equation of Von Hoyningen-Huene (1981). In the SWAT parameter database, the CANMX ranges from 0 to 100 mm H<sub>2</sub>O (Neitsch et al., 2011), and users may obtain particularly high fitted CANMX values. For example, Jajarmizadeh et al. (2017) obtained a fitted CANMX value of 55 in their model, Pang et al. (2020) obtained a fitted CANMX value of 40, and Mendonça dos Santos et al. (2020) obtained a fitted forest CANMX value of 80. These values are acceptable for modeling studies because less sensitive parameters may not be fully calibrated due to the algorithm in SWAT-CUP, but the model still obtains a satisfactory mathematical simulation result (Abbaspour et al., 2007). However, this value



cannot explain the actual hydrological processes in a forest or catchment because the values of the daily maximum canopy storage are too high and are nearly impossible in actual situations.

In this study, the fitted CANMX values in the Ikoma forest region were lower than those in the other three forest regions. This could either be due to uncertainty in the model or due to the actual situation in the study area. The uncertainty is based on the fact that the observation points in the catchment area cover other land use types apart from forests, which may affect the sensitivity of forest CANMX parameters. Compared to previous research, Syahida and Azida (2018) measured canopy intercept using a rainfall simulator and showed that a coniferous vegetation canopy can generally intercept more precipitation. Saito et al. (2013) measured the canopy interception rates of *Cryptomeria japonica* and *Chamaecyparis obtuse* in Japan, both of which were 25.5%. Hörmann et al. (1996) and Fathizadeh et al. (2013) measured the canopy interception rates of *Quercus serrata* in Germany and Iran, both of which were only 20%. Based on these findings, we think that the SWAT results for CANMX obtained in this study are reasonable.

Another uncertainty lies in the transpiration calculation. We selected an LAI of 3 as the  $T$  and  $E_s$  dividing line because the SWAT algorithm also uses an LAI of 3 to calculate the transpiration ratio in its ET calculation (Neitsch et al., 2011). However, it may differ from the ground truth. In the SWAT algorithm, this part of the algorithm is skipped if the Penman–Monteith ET equation is selected as the ET method. In the Penman–Monteith equation, the vegetation canopy influence is calculated as the canopy resistance, and  $T$  cannot be separated from ET (Monteith, 1965). The Hargreaves equation only considers precipitation and temperature, but this method is not suitable unless the climate data are limited (Hargreaves et al., 1985). Priestley and Taylor (1972) also developed a popular ET estimation method, but this method does not consider wind speed and is therefore unsuitable for highly advective conditions, whereas most coastal catchments exhibit highly advective conditions. As a result, the  $E_s$  primarily covered by evergreen vegetation was very small, which may be because we ignored

$E_s$  when the LAI exceeded 3. Kunert et al. (2015) measured soil evaporation values of 0 in a well-developed evergreen forest, which is similar to the findings of this study.

#### 4.2 Forest growth and its catchment-scale impacts

In this study, the impacts of forest growth on ET in the Ikoma and Sakurai forest regions were significantly stronger than in the other forest regions, as the average tree ages in these two forest regions were younger. Molchanov (1963) summarized the relationship between forest ET and average tree ages, and found that ET increased with increasing tree ages in forests that contained trees less than 50 years old. This is consistent with the performance of the Ikoma and Sakurai forest areas in this study. However, Molchanov (1963) also noted that forests with trees greater than 50 years old exhibit decreased ET with plant growth, which was not confirmed in the current study. There are two potential reasons for this. This type of forest evapotranspiration study is usually accomplished by investigating forests of different ages during the same period and cannot reflect continuous long-term forest growth processes (Molchanov, 1963, Murakami, 2002). More importantly, as mentioned above, the continued increases in atmospheric CO<sub>2</sub> concentrations since the 1980s have enhanced plant growth (Nemani et al., 2003). This is supported by the observed increases in CO<sub>2</sub> mixing ratio during the 1990s in Central Japan (Inoue and Matsueda, 2001). As the average age of the trees is older, the LAI did not increase significantly during the 40 year study period in the Kasuga and Kongo forest regions, which is consistent with the growth characteristics of trees in previous studies (Molchanov, 1963, Liu et al., 2012). Due to these atmospheric changes, the growth of forests resulted in slight increases in ET. In contrast, due to the young tree ages and good management strategies in the Ikoma and Sakurai forest regions, atmospheric changes more obviously intensified the forest growth process during the growth phase, which has led to significant increases in ET.

Three of the forest regions in this study were "mixed forests;" however, both the canopy

characteristics and water balance for each forest region during each period differed. The Ikoma region, which exhibited high deciduous vegetation coverage, also generated the most surface runoff of the four forest regions (Figure 6). Thus, the ratio of deciduous and evergreen vegetation communities in the mixed forest exerted a major influence on the terrestrial hydrological processes.

For mixed land use catchments, such as urbanized catchments, forests are typically located upstream of the catchment and cover a large area. The water yield of forests directly affects the downstream catchment, which is typically covered by residential areas. High-density forests contribute less baseflow, while low-density forests contribute a larger quantity of the baseflow. If the actual forest growth scenario is not considered, the baseflow and river discharge of the catchment may be overestimated or underestimated. In extreme cases, unrealistic forest growth conditions may lead to unpredictable downstream droughts or floods due to the overestimation or underestimation of upstream baseflow discharge. There are many cases of regulating downstream water hazards by adjusting the upstream forest density, which requires accurate quantifications and analyses of forest growth and its hydrologic impacts (Komatsu et al., 2010; Ford et al., 2011). In addition, attention should be paid to forest growth in studies of long-term land use changes. Suttles et al. (2018) demonstrated that land use changes impact baseflow more severely than climate change. However, their study did not consider forest growth. Forest growth can reduce baseflow and can be superimposed on the impact of land use changes, which can further reduce the baseflow and cause a drought (Gaertner et al., 2019). If the forest is over-felled, the forest density is reduced and a larger water yield from the upstream area may cause downstream flooding.

## 5. Conclusions

We conducted a study of the detailed temporal evolution of forest growth and its impact on the hydrological response during different periods in four forest regions with different canopy

phenology characteristics. Additionally, we designed a method to separate canopy evaporation and transpiration, soil evaporation, and the understory vegetation evapotranspiration, from the SWAT results. The method to quantify forest density changes through long-term LAI changes and LAI phenological changes, as well as the method of separating the ET processes can be used widely for other catchments and is not limited by data availability. We found that the water balance of different mixed forests with different vegetation community compositions under different growth conditions was very different. In addition, the most significant change we observed was the increase in canopy evaporation that accompanied increases in forest and canopy density. Under influence of changes in the atmospheric environment and forest management policies, the hydrological and ecological environment of the forest is changing. The results of this study emphasize that forest characteristics and parameters used in long-term studies require adjustments based on ground truthed data. Accurate quantifications of the upstream forest characteristics and water balance are crucial for understanding the downstream water environment, ignoring the vegetation proportions in forests and their growth characteristics and changes produces inaccurate forest ET estimates, thereby yielding incorrect estimated of the distribution of forest and downstream catchment water resources. The results of this study provide valuable information for SWAT and hydrological modeling that can be used to accurately assess the hydrological and ecological cycles of forests and complex watersheds, particularly for detailed ET processes. Finally, we encourage the model users to estimate the range of parameters through the methods described in this paper, or other feasible methods, before calibrating the canopy storage parameters to improve the practical significance of the parameter.

*Corresponding Author:*

Shin-ichi Onodera

Graduate School of Advanced Science and Engineering, Hiroshima University

1-7-1 Kagamiyama, Higashi-Hiroshima, 7398521, Japan

-81-824-24-6496

sonodera@hiroshima-u.ac.jp

*Acknowledgment*

We thank the suggestions from Dr. Takanori Shimizu, Dr. Masahiro Kobayashi and Dr. Naohiro Imamura for their comments. This material is based on work supported by the Asia-Pacific Network for Global Change Research (APN) under Grant No. CRRP2019-09MY-Onodera (funder ID: <http://dx.doi.org/10.13039/100005536>). Research promotion for the environmental creation and rehabilitation of Osaka Bay area by Osaka Bay Regional Offshore Environmental Improvement Center (Project No. 010005, PI: Mitsuyo Saito). And Grant-in-Aid for Scientific Research (A) by Japan Society for the Promotion of Science (Project No. 18H04151, PI: Shin-ichi Onodera)

*Data statement*

The data that support the findings of this study are available from the corresponding author, upon reasonable request.

**References**

- Abbaspour, K. C., Vejdani, M., Haghighat, S., & Yang, J. (2007). SWAT-CUP calibration and uncertainty programs for SWAT. In MODSIM 2007 international congress on modelling and simulation, modelling and simulation society of Australia and New Zealand (pp. 1596-1602).
- Agriculture and forestry department of Nara, (2018). Nara Forestry Statistics Report 2016. <http://www.pref.nara.jp/1218.htm>
- Alemayehu, T., Griensven, A. V., Woldegiorgis, B. T., & Bauwens, W. (2017). An improved SWAT vegetation growth module and its evaluation for four tropical ecosystems. *Hydrology and Earth System Sciences*, 21(9), 4449-4467.
- Dube, T., Mutanga, O., Sibanda, M., Shoko, C., & Chemura, A. (2017). Evaluating the influence of the Red Edge band from RapidEye sensor in quantifying leaf area index for hydrological applications specifically focussing on plant canopy interception. *Physics and Chemistry of the Earth, Parts A/B/C*, 100, 73-80.
- Durlo, G., Jagiełło-Leńczuk, K., Małek, S., Banach, J., Dudek, K., & Kormanek, M. (2016). Hydrological responses to

- forest cover change in mountains under projected climate conditions. *International Journal of Environmental & Agriculture Research*, 2(10), 60-68.
- FAO (2020). Global Forest Resources Assessment 2020: Main report. Rome. <https://doi.org/10.4060/ca9825en>
- Fathizadeh, O., Attarod, P., Pypker, T. G., Darvishsefat, A. A., & Zahedi Amiri, G. H. (2013). Seasonal variability of rainfall interception and canopy storage capacity measured under individual oak (*Quercus brantii*) trees in Western Iran. *Journal of Agricultural Science and technology*, 15(1), 175-188.
- Ford, C. R., Laseter, S. H., Swank, W. T., & Vose, J. M. (2011). Can forest management be used to sustain water - based ecosystem services in the face of climate change?. *Ecological Applications*, 21(6), 2049-2067.
- Gaertner, B. A., Zegre, N., Warner, T., Fernandez, R., He, Y., & Merriam, E. R. (2019). Climate, forest growing season, and ET changes in the central Appalachian Mountains, USA. *Science of The Total Environment*, 650, 1371-1381.
- Gupta HV, Sorooshian S, Yapo PO (1998) Toward improved calibration of hydrologic models: Multiple and noncommensurable measures of information. *Water Resources Research* 34: 751-763.
- Hargreaves, G.L., Hargreaves, G.H., Riley, J.P., (1985). Agricultural benefits for Senegal River basin. *Journal of irrigation and Drainage Engineering* 111: 113-124. *KSCE Journal of Civil Engineering* (2010) 14(6):931-939. DOI 10.1007/s12205-010-0851-8
- Hörmann, G., Branding, A., Clemen, T., Herbst, M., Hinrichs, A., & Thamm, F. (1996). Calculation and simulation of wind controlled canopy interception of a beech forest in Northern Germany. *Agricultural and Forest Meteorology*, 79(3), 131-148.
- Inoue, H. Y., & Matsueda, H. (2001). Measurements of atmospheric CO<sub>2</sub> from a meteorological tower in Tsukuba, Japan. *Tellus B*, 53(3), 205-219.
- Jajarmizadeh, M., Sidek, L. M., Harun, S., & Salarpour, M. (2017). Optimal calibration and uncertainty analysis of SWAT for an arid climate. *Air, Soil and Water Research*, 10, 1178622117731792.
- Japan foreststock association (2021). Mt. Kongo Chihayaakasaka Village Michida Forest. <http://www.foreststock.or.jp/forests/michidaringyo2/>
- Kayane I, Takeuchi A (1971) On the Annual Runoff Ratio of Japanese Rivers (in Japanese). *Geographical Review*, 44-5, 1971
- Komatsu, H., Tanaka, N., & Kume, T. (2007). Do coniferous forests evaporate more water than broad-leaved forests in Japan? *Journal of Hydrology*, 336(3-4), 361-375.
- Komatsu, H., Kume, T., & Otsuki, K. (2008). The effect of converting a native broad-leaved forest to a coniferous plantation forest on annual water yield: a paired-catchment study in northern Japan. *Forest Ecology and Management*, 255(3-4), 880-886.
- Komatsu, H., Kume, T., & Otsuki, K. (2009). Changes in low flow with the conversion of a coniferous plantation to a broad - leaved forest in a summer precipitation region, Japan. *Ecohydrology: Ecosystems, Land and Water Process Interactions, Ecohydrogeomorphology*, 2(2), 164-172.
- Komatsu, H., Kume, T., & Otsuki, K. (2010). Water resource management in Japan: Forest management or dam

- reservoirs?. *Journal of environmental management*, 91(4), 814-823.
- Kozak, J. A., Ahuja, L. R., Green, T. R., & Ma, L. (2007). Modelling crop canopy and residue rainfall interception effects on soil hydrological components for semi - arid agriculture. *Hydrological Processes: An International Journal*, 21(2), 229-241.
- Kunert, N., Aparecido, L. M. T., Barros, P., & Higuchi, N. (2015). Modeling potential impacts of planting palms or tree in small holder fruit plantations on ecohydrological processes in the Central Amazon. *Forests*, 6(8), 2530-2544.
- Kvalseth, T.O., (1985). Cautionary Note about R2, *The American Statistician* Vol. 39, No. 4, Part 1 (Nov., 1985), pp. 279-285
- Liu, Y., Liu, R., & Chen, J. M. (2012). Retrospective retrieval of long - term consistent global leaf area index (1981–2011) from combined AVHRR and MODIS data. *Journal of Geophysical Research: Biogeosciences*, 117(G4).
- MacDicken, K., Jonsson, Ö., Piña, L., Maulo, S., Contessa, V., Adikari, Y., ... & D'Annunzio, R. (2016). Global forest resources assessment 2015: how are the world's forests changing?
- Marhaento, H., Booij, M. J., Rientjes, T. H. M., & Hoekstra, A. Y. (2017). Attribution of changes in the water balance of a tropical catchment to land use change using the SWAT model. *Hydrological processes*, 31(11), 2029-2040.
- Mendonça dos Santos, F., Proença de Oliveira, R., & Augusto Di Lollo, J. (2020). Effects of Land Use Changes on Streamflow and Sediment Yield in Atibaia River Basin—SP, Brazil. *Water*, 12(6), 1711.
- Molchanov, A. A. (1963). The hydrological role of forests. *The hydrological role of forests*.
- Monteith, J., (1965). Evaporation and environment. *Symp Soc Exp Biol*, p: 4.
- Moriasi, D.N., Arnold, J.G., Van Liew, M.W., Bingner, R.L., Harmel, R.D., Veith, T.L. (2007). Model evaluation guidelines for systematic quantification of accuracy in watershed simulations. *Transactions of the ASABE*. 50(3):885-900
- Murakami S. (2002) Dependency of LAI and Evapotranspiration on Stand Age at Planted Stands of Japanese Cypress (*Chamaecyparis obtusa*) and Cedar (*Cryptomeria japonica*) and its Potential for the Application to the Management of Water Conservation Forest (in Japanese). *J. Japan Soc. Hydrol. & Water Resour.*, 15(5), 461-471.
- Myneni, R., Knyazikhin, Y., Park, T. (2015). MCD15A2H MODIS/Terra+Aqua Leaf Area Index/FPAR 8-day L4 Global 500m SIN Grid V006. NASA EOSDIS Land Processes DAAC.  
<http://doi.org/10.5067/MODIS/MCD15A2H.006>
- Nara Prefecture (2016). Kasugayama Primeval Forest Conservation Plan
- Nara Prefecture (2021). Trees' story in Nara. <https://www3.pref.nara.jp/naranoki/about/>
- Nash, J., Sutcliffe, J.V., (1970). River flow forecasting through conceptual models' part I-A discussion of principles. *Journal of Hydrology* 10, 282-290
- Neitsch, S. L., Arnold, J. G., Kiniry, J. R., & Williams, J. R. (2011). Soil and water assessment tool theoretical documentation version 2009. Texas Water Resources Institute.

- Nemani, R. R., Keeling, C. D., Hashimoto, H., Jolly, W. M., Piper, S. C., Tucker, C. J., ... & Running, S. W. (2003). Climate-driven increases in global terrestrial net primary production from 1982 to 1999. *science*, 300(5625), 1560-1563.
- Nepstad, D. C., de Carvalho, C. R., Davidson, E. A., Jipp, P. H., Lefebvre, P. A., Negreiros, G. H., et al., (1994). The role of deep roots in the hydrological and carbon cycles of Amazonian forests and pastures. *Nature*, 372(6507), 666.
- Omer, A., Zhuguo, M., Zheng, Z., & Saleem, F. (2020). Natural and anthropogenic influences on the recent droughts in Yellow River Basin, China. *Science of The Total Environment*, 704, 135428.
- Osaka Prefecture (2021). History of Ikoma forests. [https://www.pref.osaka.lg.jp/chubunm/chubu\\_nm/ryokuti17.html](https://www.pref.osaka.lg.jp/chubunm/chubu_nm/ryokuti17.html)
- Osman, N., & Barakbah, S. S. (2006). Parameters to predict slope stability—soil water and root profiles. *Ecological Engineering*, 28(1), 90-95.
- Quéré, C. L., Moriarty, R., Andrew, R. M., Canadell, J. G., Sitch, S., Korsbakken, J. I., ... & Zeng, N. (2015). Global carbon budget 2015. *Earth System Science Data*, 7(2), 349-396.
- Pang, S., Wang, X., Melching, C. S., & Feger, K. H. (2020). Development and testing of a modified SWAT model based on slope condition and precipitation intensity. *Journal of Hydrology*, 588, 125098.
- Parajuli, P. B., Jayakody, P., & Ouyang, Y. (2018). Evaluation of using remote sensing ET data in SWAT. *Water resources management*, 32(3), 985-996.
- Paul-Limoges, E., Wolf, S., Schneider, F. D., Longo, M., Moorcroft, P., Gharun, M., & Damm, A. (2020). Partitioning ET with concurrent eddy covariance measurements in a mixed forest. *Agricultural and Forest Meteorology*, 280, 107786.
- Priestley, C. & Taylor, R., (1972). On the assessment of surface heat flux and evaporation using large-scale parameters. *Monthly Weather Review* 100: 81-92.
- Qin, Y. M., Xu, Y. L., Li, H. E. (2009). SWAT model of non-point source pollution under different land use scenarios in the Heihe river basin (in Chinese). *Acta scientiae Circumstantiae*, 29(2):440-448.
- Rautiainen, A., Wernick, I., Waggoner, P. E., Ausubel, J. H., & Kauppi, P. E. (2011). A national and international analysis of changing forest density. *PLoS one*, 6(5), e19577.
- Running, S. W., Mu, Q., Zhao, M., & Moreno, A. (2019). MODIS Global Terrestrial ET (ET) Product (MOD16A2/A3 and Year-end Gap-filled MOD16A2GF/A3GF) NASA Earth Observing System MODIS Land Algorithm (For Collection 6).
- Saito, T., Matsuda, H., Komatsu, M., Xiang, Y., Takahashi, A., Shinohara, Y., & Otsuki, K. (2013). Forest canopy interception loss exceeds wet canopy evaporation in Japanese cypress (Hinoki) and Japanese cedar (Sugi) plantations. *Journal of Hydrology*, 507, 287-299.
- Sharma, K., & Saikia, A. (2018). How green was my valley: forest canopy density in relation to topography and anthropogenic effects in Manipur valley, India. *Geografisk Tidsskrift-Danish Journal of Geography*, 118(2), 137-150.
- Skovsgaard, J. P., Bald, C., & Nord-Larsen, T. (2011). Functions for biomass and basic density of stem, crown and root



- system of Norway spruce (*Picea abies* (L.) Karst.) in Denmark. *Scandinavian Journal of Forest Research*, 26(S11), 3-20.
- Sun, H., Cornish, P.S., (2005). Estimating shallow groundwater recharge in the headwaters of the Liverpool Plains using SWAT. *Hydrological Process*. 19, 795–807 (2005)
- Suttles, K. M., Singh, N. K., Vose, J. M., Martin, K. L., Emanuel, R. E., Coulston, J. W., ... & Crump, M. T. (2018). Assessment of hydrologic vulnerability to urbanization and climate change in a rapidly changing watershed in the Southeast US. *Science of the Total Environment*, 645, 806-816.
- Soil Conservation Service Engineering Division. (1986). *Urban hydrology for small watersheds*. U.S. Department of Agriculture, Technical Release 55.
- Staelens, J., Herbst, M., Hölscher, D., & De Schrijver, A. (2011). Seasonality of hydrological and biogeochemical fluxes. In *Forest Hydrology and Biogeochemistry* (pp. 521-539). Springer, Dordrecht.
- Swank, W.T.& Douglass, J.E., (1974). Streamflow greatly reduced by converting deciduous hardwood stands to pine. *Science* 185,857–859.
- Syahida, A. N., & Azida, A. A. (2018). The effect of vegetation canopy on canopy storage capacity with different rainfall intensity. In *MATEC Web of Conferences* (Vol. 250, p. 04001). EDP Sciences.
- Takeda, I., Fukushima, A., & Somura, H. (2010). Characteristics of Hydrological Runoff in an Artificial Coniferous Forest with Delayed Thinning and Its Long-term Changes. *TJSID*, 77(5), 509-516.
- Tomimura environmental office (2015). *Michida forestry forest sink and biodiversity Report*.
- USDA (1980). *CREAMS, A Field Scale Model for Chemicals, Runoff, and Erosion from Agricultural Management Systems*. Conservation research report No.26.USDA, Washing, D.C.1980:643~644
- Von Hoyningen-Huene J. (1981). *Die Interzeption Des Niederschlags in landwirtschaftlichen Pflanzenbeständen* (in German). *Arbeitsbericht Deutscher Verband für Wasserwirtschaft und Kulturbau*, DVWK, Braunschwig, Germany
- Wang, K., Onodera, S. I., Saito, M., & Shimizu, Y. (2021). Long-term variations in water balance by increase in percent imperviousness of urban regions. *Journal of Hydrology*, 602, 126767. [doi.org/10.1016/j.jhydrol.2021.126767](https://doi.org/10.1016/j.jhydrol.2021.126767)
- Zhao, J., Xu, C. C., Gao, S. T., & Li, J. X. (2015). Hydrological modeling in the Urumqi River basin based on SWAT (in Chinese). *Arid Land Geogr*, 38(4), 666-674.

Table 1. Calibrated plant database parameters used in this study

Name	Describe	Ikoma	Kasuga	Kongo	Sakurai
FRGRW1	Fraction of the plant growing season corresponding to the 1 <sup>st</sup> point on the optimal leaf area development curve.	0.40	0.38	0.38	0.37
LAIMX1	Fraction of the maximum leaf area index corresponding to the 1 <sup>st</sup> point on the optimal leaf area development curve.	0.10	0.15	0.15	0.20
FRGRW2	Fraction of the plant growing season corresponding to the 2 <sup>nd</sup> point on the optimal leaf area development curve.	0.55	0.53	0.53	0.37
LAIMX2	Fraction of the maximum leaf area index corresponding to the 2 <sup>nd</sup> point on the optimal leaf area development curve.	0.70	0.85	0.85	0.90
T_OPT	Optimal temperature for plant growth (°C)	28	26	26	26
T_BASE	Minimum temperature for plant growth (°C)	5	5	5	5
CHTMX	Maximum canopy height (m)	30	30	30	30
CN2a	SCS runoff curve number (Hydrologic group: A)	35	26	24	21
CN2b	SCS runoff curve number (Hydrologic group: B)	54	49	48	46
CN2c	SCS runoff curve number (Hydrologic group: C)	64	61	60	59
CN2d	SCS runoff curve number (Hydrologic group: D)	69	67	66	65

Table 2. Model efficiency coefficients

Period	Target	Calibration / Validation	R <sup>2</sup>	NSE	PBIAS
2010s	LAI (Ikoma)	2017 (calibration) / 2018 (validation)	0.97 / 0.94	0.95 / 0.93	-1.51 / -1.68
	LAI (Kasuga)	2017 (calibration) / 2018 (validation)	0.93 / 0.93	0.92 / 0.90	-1.22 / -1.85
	LAI (Kongo)	2017 (calibration) / 2018 (validation)	0.95 / 0.91	0.93 / 0.89	-1.47 / -1.91
	LAI (Sakurai)	2017 (calibration) / 2018 (validation)	0.94 / 0.92	0.93 / 0.91	-0.45 / -0.76
	ET (Ikoma)	2009–2013 (GC/SC) / 2014–2018 (GC/SV)	0.92 / 0.89	0.91 / 0.87	-3.0 / -3.6
	ET (Kasuga)	2009–2013 (GC/SC) / 2014–2018 (GC/SV)	0.91 / 0.88	0.90 / 0.86	-2.2 / -4.3
	ET (Kongo)	2009–2013 (GC/SC) / 2014–2018 (GC/SV)	0.91 / 0.87	0.90 / 0.85	-3.8 / -4.3
	ET (Sakurai)	2009–2013 (GC/SC) / 2014–2018 (GC/SV)	0.93 / 0.85	0.92 / 0.83	-2.0 / -4.7
	SF (Banjou)	2009–2013 (GC/SC) / 2014–2018 (GC/SV)	0.73 / 0.67	0.72 / 0.67	4.6 / 5.7
	SF (Hota)	2009–2013 (GC/SC) / 2014–2018 (GC/SV)	0.69 / 0.64	0.67 / 0.62	7.6 / 11.5
	SF (Ouji)	2009–2013 (GC/SC) / 2014–2018 (GC/SV)	0.86 / 0.78	0.79 / 0.70	3.9 / 6.4
	SF(Kashiwara)	2009–2013 (GC/SC) / 2014–2018 (GC/SV)	0.93 / 0.89	0.92 / 0.89	2.1 / 4.7
2000s	SF (Banjou)	1999–2003 (GV/SC) / 2004–2008 (GV/SV)	0.88 / 0.82	0.76 / 0.69	9.7 / 13.6
	SF (Hota)	1999–2003 (GV/SC) / 2004–2008 (GV/SV)	0.67 / 0.62	0.61 / 0.58	10.3 / 14.7
	SF (Ouji)	1999–2003 (GV/SC) / 2004–2008 (GV/SV)	0.93 / 0.89	0.81 / 0.77	9.6 / 12.3
	SF(Kashiwara)	1999–2003 (GV/SC) / 2004–2008 (GV/SV)	0.94 / 0.90	0.86 / 0.85	8.0 / 10.3
1990s	SF (Banjou)	1989–1993 (GV/SC) / 1994–1998 (GV/SV)	0.94 / 0.91	0.72 / 0.66	9.9 / 13.1
	SF (Hota)	1989–1993 (GV/SC) / 1994–1998 (GV/SV)	0.71 / 0.61	0.57 / 0.53	10.0 / 14.8
	SF (Ouji)	1989–1993 (GV/SC) / 1994–1998 (GV/SV)	0.94 / 0.93	0.88 / 0.84	8.4 / 11.6
	SF(Kashiwara)	1989–1993 (GV/SC) / 1994–1998 (GV/SV)	0.95 / 0.93	0.90 / 0.91	8.7 / 10.9
1980s	SF (Banjou)	1979–1983 (GV/SC) / 1984–1988 (GV/SV)	0.81 / 0.72	0.59 / 0.57	12.6 / 14.7
	SF (Hota)	1979–1983 (GV/SC) / 1984–1988 (GV/SV)	0.73 / 0.69	0.62 / 0.59	10.9 / 12.5
	SF (Ouji)	1979–1983 (GV/SC) / 1984–1988 (GV/SV)	0.96 / 0.89	0.83 / 0.77	9.6 / 13.5
	SF(Kashiwara)	1979–1983 (GV/SC) / 1984–1988 (GV/SV)	0.93 / 0.9	0.88 / 0.78	8.3 / 9.9

(SF: Streamflow; GC: global calibration; SC: sub-calibration; GV: global validation; SV: sub-validation)

Table 3. Canopy density parameters and fitted CANMX values during different periods

Type	Name	Describe	Scale	1980s	1990s	2000s	2010s
Input value	LAI_INIT	Initial LAI	Ikoma	0.7	0.7	0.9	0.9
			Kasuga	2.9	3.1	3.3	3.2
			Kongo	2.7	2.9	2.9	2.6
			Sakurai	2.6	3.0	3.5	4.0
	ALAI_MIN	Minimum LAI for plants during dormant period	Ikoma	0.7	0.7	0.9	0.9
			Kasuga	2.9	3.1	3.3	3.2
			Kongo	2.7	2.9	2.9	2.6
			Sakurai	2.6	3.0	3.5	4.0
	BLAI	Maximum potential LAI	Ikoma	3.9	4.9	5.9	6.5
			Kasuga	5.3	5.7	6.0	5.9
			Kongo	4.9	5.1	5.1	4.7
			Sakurai	3.7	4.4	5.1	5.7
Fitted value	CANMX	Maximum canopy storage (mm)	Ikoma	1.43	1.92	2.80	3.94
			Kasuga	4.21	4.93	5.27	5.27
			Kongo	3.70	4.10	3.93	3.64
			Sakurai	2.77	3.35	4.18	4.78

Figure 1. Meteorological and hydrological station locations and watershed information

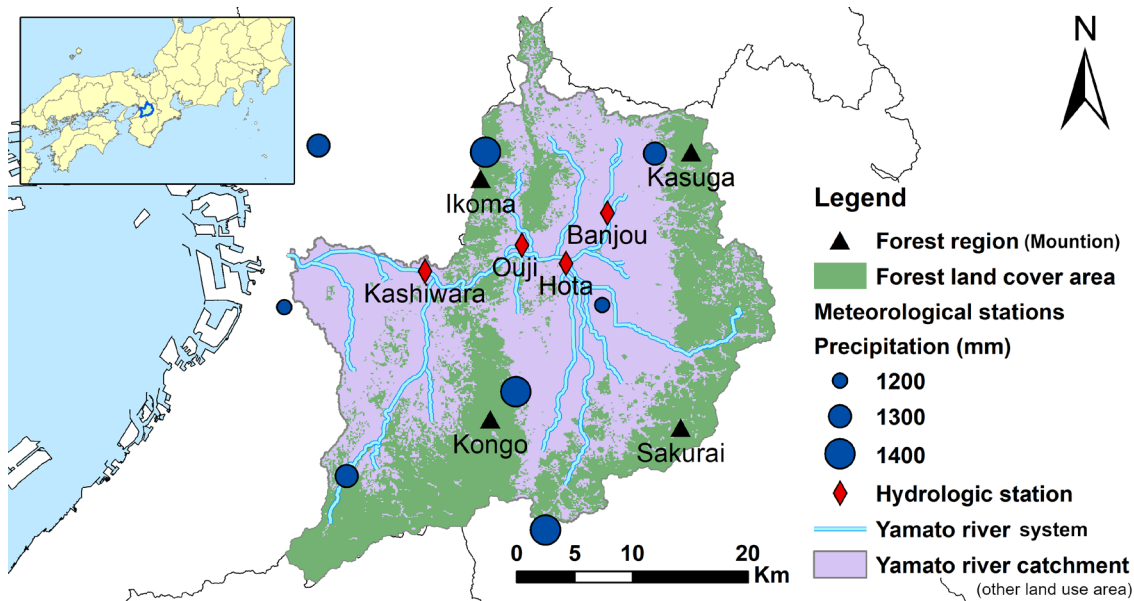


Figure 2. Fitted leaf area index (LAI) growth curves for the forest regions in the study area

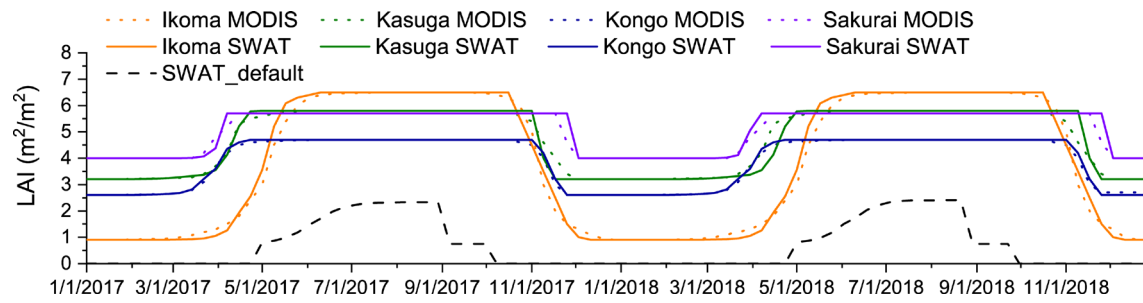


Figure 3. Comparison of MODIS ET and SWAT ET data during the global calibration period

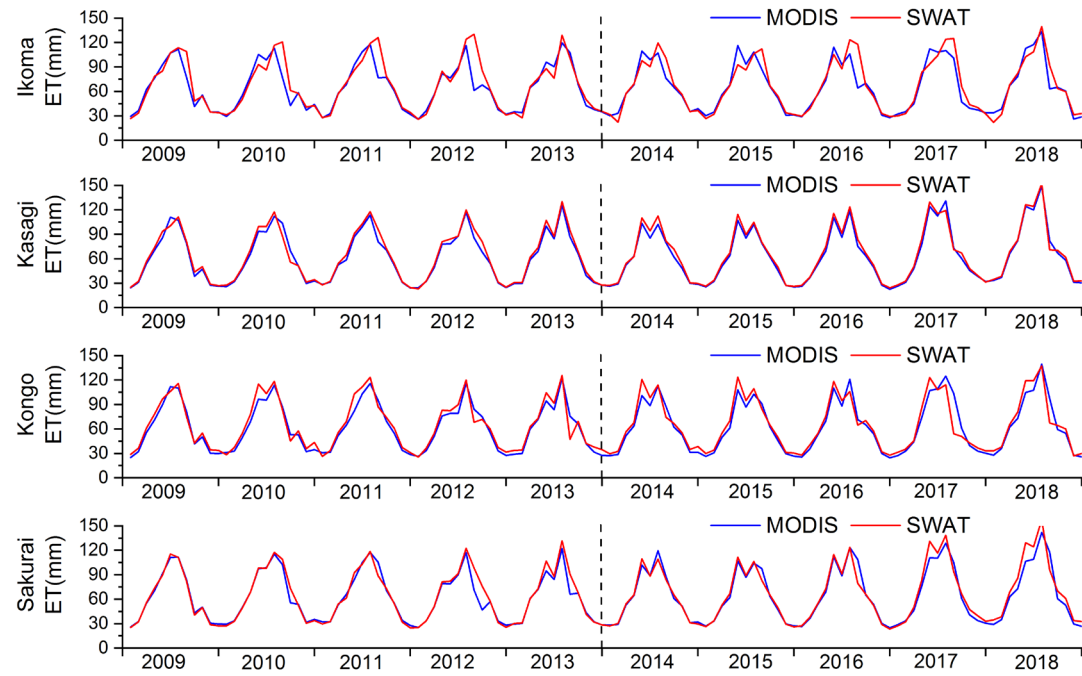


Figure 4. Monthly mean streamflow simulations at each hydrological station

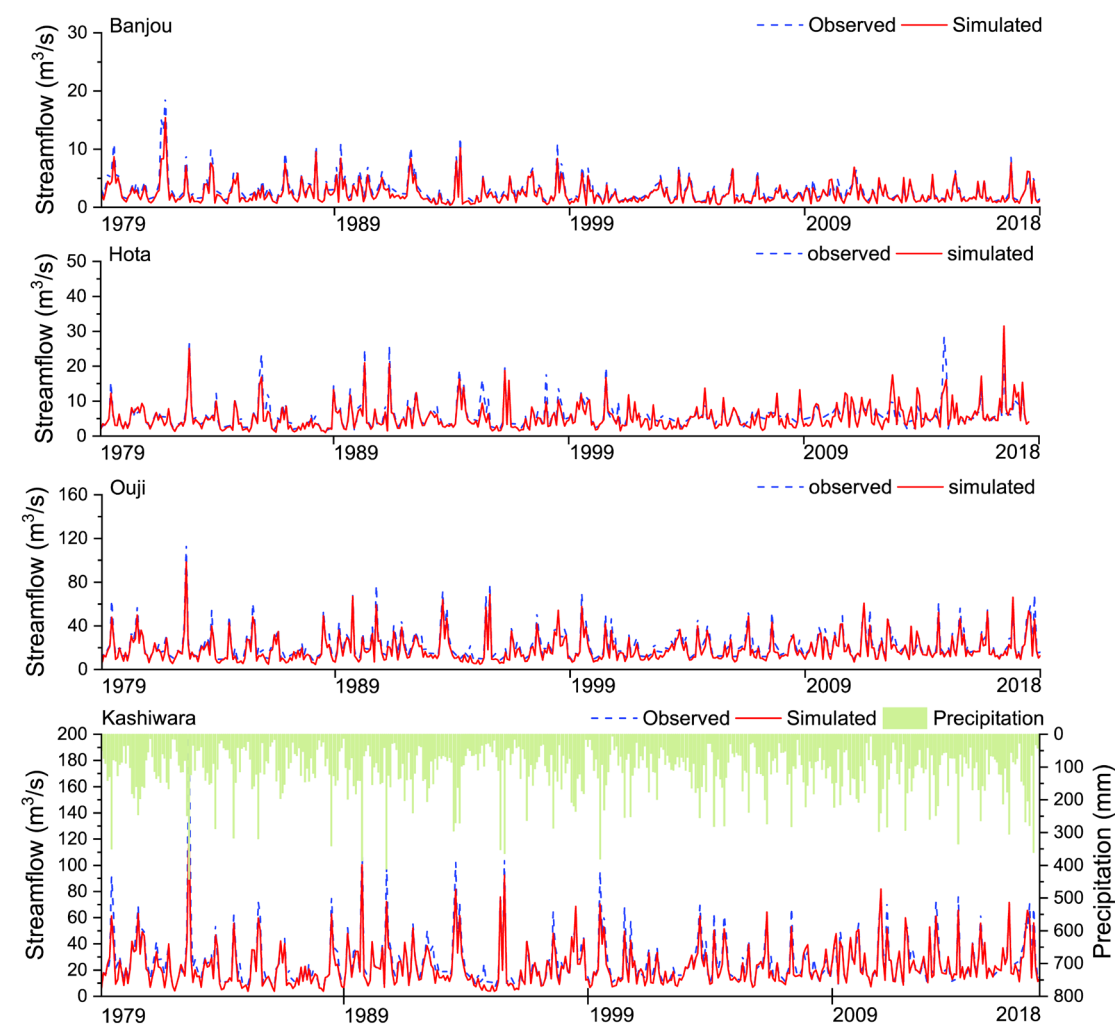




Figure 5. Changes in forest evapotranspiration (ET) processes due to forest growth

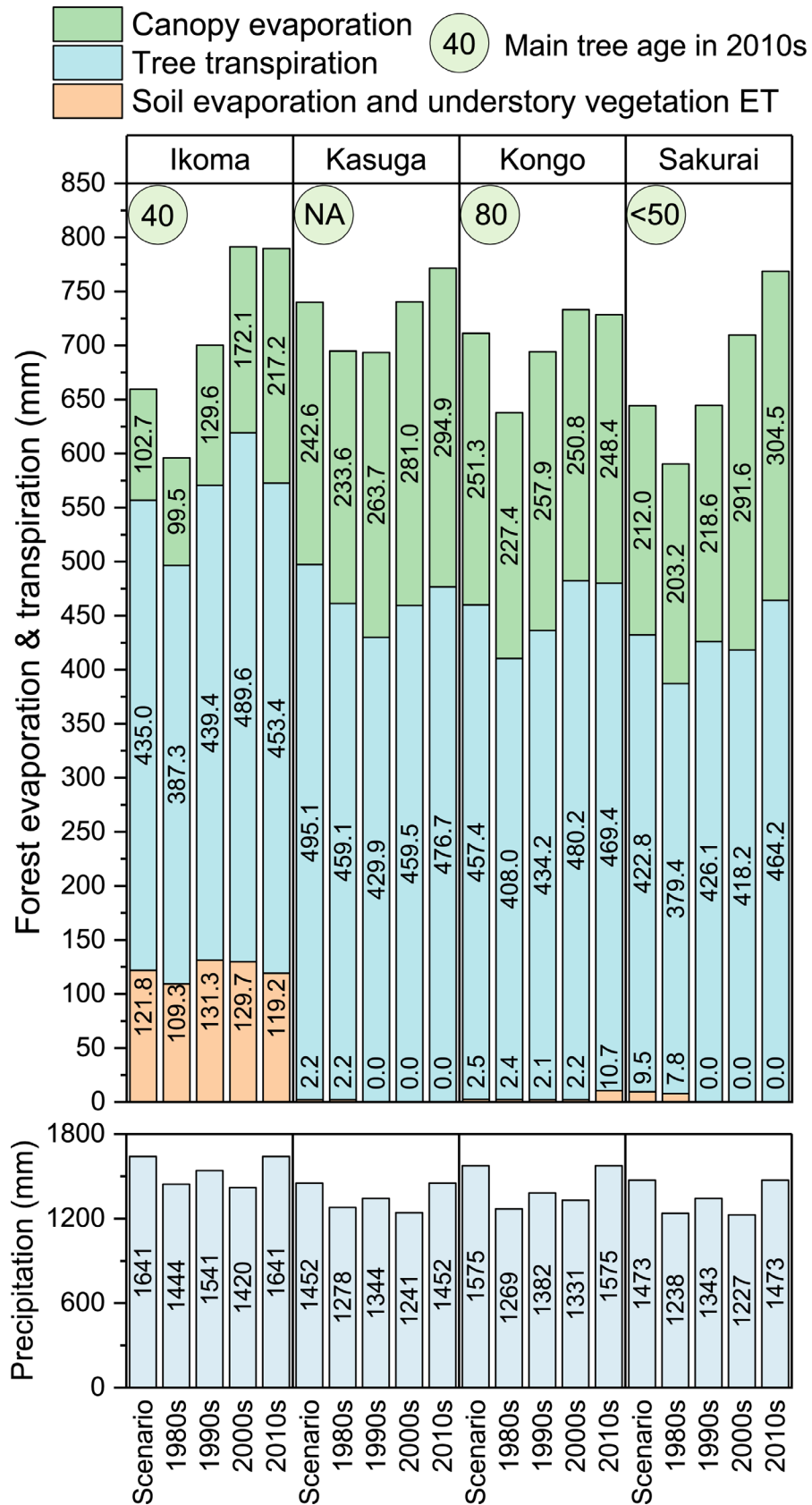


Figure 6. Surface runoff and baseflow for each region during different periods

